Retinitis pigmentosa: rapid neurodegeneration is governed by slow cell death mechanisms

Sahaboglu, A.; Paquet-Durand, O.; Dietter, J.; Dengler, K.; Bernhard-Kurz, S.; Ekström, Per; Hitzmann, B.; Ueffing, M.; Paquet-Durand, F.

Published in:
Cell Death & Disease

DOI:
10.1038/cddis.2013.12

2013

Citation: Cell Death and Disease (2013) 4, e488; doi:10.1038/cddis.2013.12

www.nature.com/cddis

Retinitis pigmentosa: rapid neurodegeneration is governed by slow cell death mechanisms

A Sahaboglu[1], O Paquet-Durand[2], J Dietter[1], K Dengler[3], S Bernhard-Kurz[1], PAR Ekström[4], B Hitzmann[2], M Ueffing[1] and F Paquet-Durand*[,1]

For most neurodegenerative diseases the precise duration of an individual cell's death is unknown, which is an obstacle when counteractive measures are being considered. To address this, we used the *rd1* mouse model for retinal neurodegeneration, characterized by phosphodiesterase-6 (PDE6) dysfunction and photoreceptor death triggered by high cyclic guanosine-mono-phosphate (cGMP) levels. Using cellular data on cGMP accumulation, cell death, and survival, we created mathematical models to simulate the temporal development of the degeneration. We validated model predictions using organotypic retinal explant cultures derived from wild-type animals and exposed to the selective PDE6 inhibitor zaprinast. Together, photoreceptor data and modeling for the first time delineated three major cell death phases in a complex neuronal tissue: (1) initiation, taking up to 36 h, (2) execution, lasting another 40 h, and finally (3) clearance, lasting about 7 h. Surprisingly, photoreceptor neurodegeneration was noticeably slower than necrosis or apoptosis, suggesting a different mechanism of death for these neurons.

Cell Death and Disease (2013) **4,** e488; doi:10.1038/cddis.2013.12; published online 7 February 2013
Subject Category: Neuroscience

Neurodegenerative diseases are an increasing health concern in the aging population, but despite massive research two fundamental questions remain: (1) what are the mechanisms of cell death governing neurodegenerative diseases? The seminal work of Kerr *et al.*[1] and the introduction of the terminal deoxynucleotidyl transferase dUTP nick end labeling (TUNEL) method[2] rapidly pinpointed apoptosis as the causative cell death pathway, although the relevance of alternative degeneration mechanisms is becoming increasingly evident.[3] (2) How long is the actual cell death process? Although sounding simple, this question has never been answered satisfactorily,[4] primarily because it is difficult to test experimentally.[5] The questions are obviously connected, not the least since different cell death pathways run on different timescales. For instance, necrosis is seen as a rapid, chaotic, and unordered destruction of the cell taking between a few minutes to 1–2 h to complete,[3] whereas apoptosis refers to a comparatively slow, program driven, and orderly cellular disintegration that may take 6–18 h to complete.[6,7] Knowledge on the time course of cell death will define the window-of-opportunity and may thus strongly influence future therapeutic strategies.

To follow cell death, from the first symptoms to the disappearance of a cell, requires sophisticated long-term, live-tissue imaging technology.[5] Yet, previous *in vivo* imaging experiments[8] could not determine the precise time frame for cell death, mainly because markers for the beginning of cellular deterioration were lacking, and most knowledge on cell death duration hence comes from dissociated cell cultures.[9] The use of intact neuronal tissues for *ex vivo* analyses presents an alternative and such studies have focused on the late phases of cell death, identified by pyknosis or DNA fragmentation (DAPI or TUNEL staining, respectively) to resolve the time a dying cell takes to completely disappear. This 'clearance time' was suggested to range from 1 to 5 h in different models for neurodegeneration.[7,10] However, as pathological alterations in DNA and nuclear structure are detectable only toward the end of the cell death process, the clearance time does not indicate how much time any affected cell has spent going from the initiation to the very end.

We set out to study the duration of neuronal cell death, using the *rd1* mouse, a homologous animal model for retinitis pigmentosa (inherited retinal degeneration, RD) with an early, rapid loss of photoreceptors, the light-sensitive neurons of the retina. The *rd1* mutation leads to loss-of-activity in rod photoreceptor cyclic guanosine-mono-phosphate (cGMP) phosphodiesterase-6 (PDE6)[11] and an accumulation of cGMP, triggering cell death.[12,13] The mechanisms behind hereditary photoreceptor neurodegeneration as such are unsettled and have been suggested to involve apoptosis,[14] necrosis,[15] as well as non-apoptotic cell death.[16] Neuronal degeneration models – including the *rd1* mouse – often exhibit

[1]Institute for Ophthalmic Research, University of Tübingen, Tübingen, Germany; [2]Institute of Food Science and Biotechnology, University of Stuttgart Hohenheim, Stuttgart, Germany; [3]Skin Clinic, University of Tübingen, Tübingen, Germany and [4]Department of Clinical Sciences, Lund, University of Lund, Lund, Sweden
*Corresponding author: F Paquet-Durand, Institute for Ophthalmic Research, University of Tübingen, Röntgenweg 11, Tübingen 72076, Germany. Tel: +49 7071 29 87430; Fax: +49 7071 29 5777; E-mail: francois.paquet-durand@klinikum.uni-tuebingen.de
Keywords: TUNEL; apoptosis; necrosis; retina; cGMP
Abbreviations: cGMP, cyclic guanosine-mono-phosphate; d, days; DPN, days post-natal; GP, glycogen phosphorylase; HDAC, histone deacetylase; ONL, outer nuclear layer; PDE6, phosphodiesterase-6; PARP, poly-ADP-ribose-polymerase; PKG, protein kinase G; RD, retinal degeneration; SQE, sum squared error; TUNEL, terminal deoxynucleotidyl transferase dUTP nick end labeling; wt, wild-type
Received 09.11.12; revised 21.12.12; accepted 03.1.13; Edited by A Verkhratsky

a constant rate of cell death, resembling the exponential decay of radioactive elements.[17,18] We built on this knowledge and used markers characteristic for different cell death stages to create a mathematical model, which for the first time allowed estimating the temporal duration of photoreceptor neurodegeneration *in vivo*. The model predictions were validated using organotypic retinal *in vitro* culture, demonstrating that the photoreceptor cell death mechanism was considerably slower than both necrosis and apoptosis.

Results

Accumulation of cGMP and photoreceptor cell death in the *rd1* retina. cGMP accumulation found in *rd1* photoreceptors is seen as the first sign of impending cellular degeneration.[13] Cell death is easily detected using the TUNEL method, which detects both necrotic and apoptotic cells.[2,19] A variety of different TUNEL-positive phenotypes were observed: some cells stained only in perinuclear areas, in others the entire nucleus was strongly positive, and yet others showed a very condensed, pyknotic, TUNEL-positive nucleus, all probably relating to different phases of cell death (Figure 1a, Supplementary Figure 1, 2). Interestingly, although high cGMP triggers TUNEL-positive *rd1* cell death,[12] cGMP did not co-label with TUNEL in photoreceptor cells (Figure 1a). Hence, cGMP and TUNEL labeled two distinct degeneration stages, separated in time by a transition period. Seen from a mechanistic point of view, PDE6 dysfunction caused a temporary rise in cGMP, followed by (yet unidentified) intermediate processes in a transition stage, before the cells turned TUNEL positive to be finally cleared away (Figure 1b). Our methodology thus provided an opportunity to study three different and temporally unique events during an individual photoreceptor cell's death.

Cellular photoreceptor cGMP accumulation (Figure 2a) was an extremely rare event in wild-type (*wt*) retina, with only few positive cells observed per retinal cross-section, in particular at early post-natal (P) days. In contrast, the number of cGMP-positive photoreceptors was significantly elevated in the outer nuclear layer (ONL) of the *rd1* retina already from P8.

The early post-natal mouse retina displays a measurable amount of developmental photoreceptor cell death,[20] seen also here by the TUNEL assay in *wt* specimens (Supplementary Figure 1A). Although *rd1* photoreceptor cell death was numerically higher at P9 when compared with *wt*, statistically significant differences were found only from P11 onward (Figure 2a).

The cGMP-dependent cell death under study was negative for caspase activity (Supplementary Figure 2) – indicating a non-apoptotic cell death mechanism – and topologically independent (i.e., no clumping of dying cells), suggesting cell-autonomous, non-necrotic processes. The delay between the significant rise of cGMP at P8, and TUNEL at P11, indicated that photoreceptor death execution could take as long as 2 to 3 days.

The percentage of cGMP-positive ONL cells in the *rd1* retina peaked at P13, coinciding with the peak of cell death (Figure 2a), after which both cGMP and TUNEL-positive cells declined, but cells with high cGMP remained more numerous than TUNEL-positive cells. As the cellular life-time of a marker determines its detection probability, these results proposed that cGMP positivity lasted longer than TUNEL positivity.

The amount of surviving photoreceptor rows showed a minor decrease in *wt* retina (because of developmental processes), whereas in *rd1* retina photoreceptor numbers strongly declined from P13 onward (Figure 2b). These data served as an index of the clearance of cells.

Modeling photoreceptor cell death kinetics. Based on the *in vivo* data on cGMP accumulation, TUNEL positivity, and survival of photoreceptors, we constructed a mathematical model for the temporal progression of neurodegeneration in the *rd1* retina (Figure 2b). We reasoned that in addition to three phases defined by cGMP, TUNEL, and clearance of cells, at least two additional transition states must exist: (1) a first one relating to unknown molecular events that, while

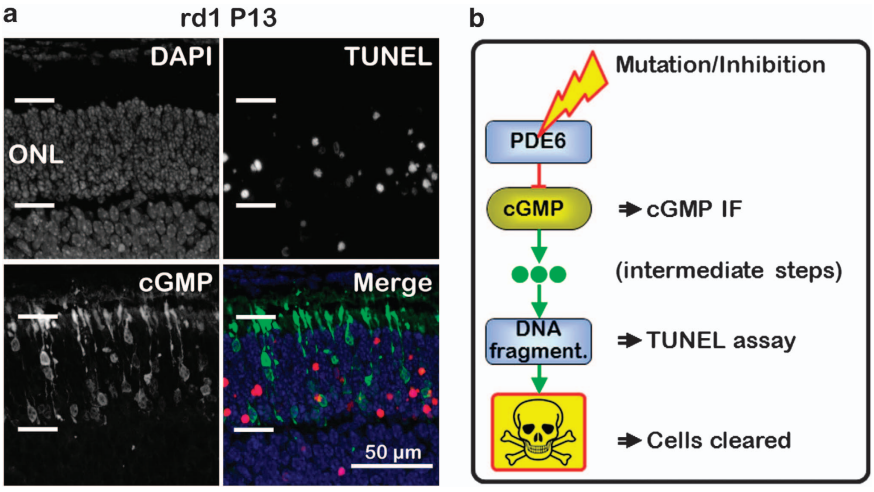

Figure 1 cGMP and photoreceptor degeneration: co-stainings in P13 *rd1* retina showed no colocalization between cGMP and TUNEL (**a**). These markers hence labeled two different stages in PDE6 dysfunction induced cell death, separated in time by a transition phase (**b**). The final clearance of cells characterizes an additional stage in cell death. Images shown are representative for at least five different *wt* and *rd1* animals

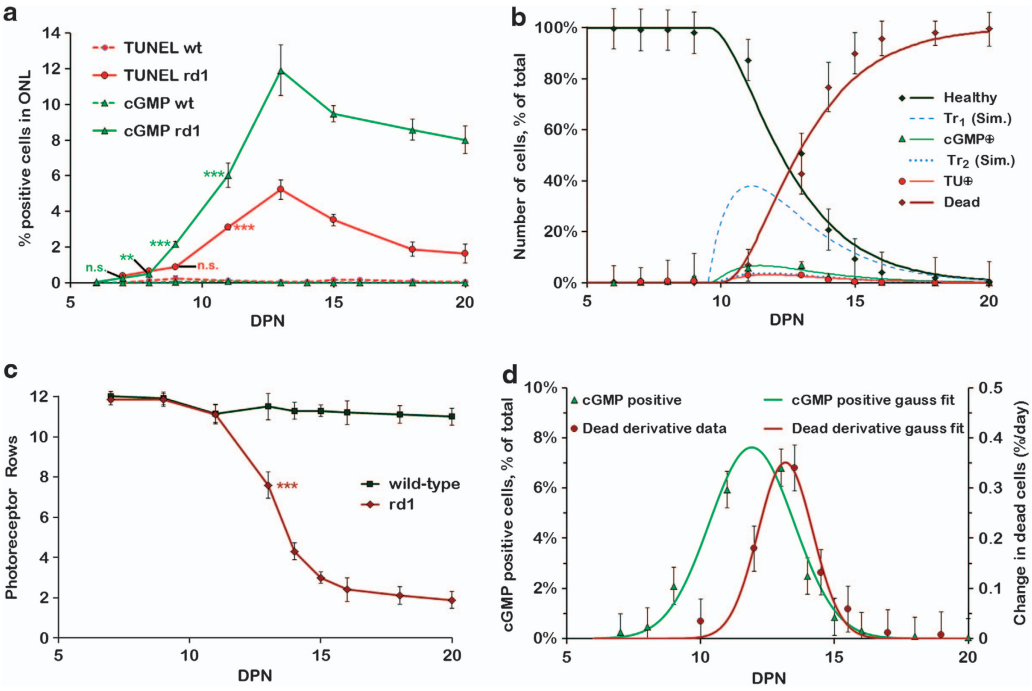

Figure 2 Progression of *rd1* photoreceptor neurodegeneration: the analysis of cellular cGMP accumulation over time (green curve in **a**) showed significant *rd1* over *wt* increases from P8 onward. The rate of cell death (red curve) rose significantly from P11 onward. Based on the *in vivo* data, a model was constructed (**b**) to simulate the temporal progression of cell death. The model accounted for six different stages (healthy, transition-1, cGMP⊕, transition-2, TUNEL⊕, and dead) each represented by a differential equation. The resulting curves are shown in (**b**) and allowed estimating the average time an individual cell needed to complete these cell death stages. Note that, since healthy cells and cells in Tr_1 are morphologically indistinguishable, the respective data sets were summed up. Increased cell death was reflected in a strong decline of surviving *rd1* photoreceptor rows (dark red curve in **c**) after P13. *Wt* retina (dark green curve) showed only a minor decrease in ONL rows because of developmental processes. In a second, independent approach, a Gauss curve was fitted to the *in vivo* cGMP⊕ data and compared with the derived *in vivo* photoreceptor survival data (**d**). The 30-h distance between the two peaks was interpreted as the average time a dying cell needs to progress from the cGMP⊕ stage to complete disappearance. Values in (**a** and **c**) represent means from $n = 3$–6 independent observations for each genotype and time point; error bars indicate S.E.M.; dotted lines in (**a**) indicate *wt* situation; DPN, days post-natal, NS, nonsignificant

cGMP negative, eventually cause unphysiologically high cGMP. (2) A second one in between cGMP and TUNEL positivity, because there was no apparent colocalization between these two markers (Figure 1a). The model also included an initial stage in which the cells were healthy. Thus, in total six different stages were considered, going from healthy (H) to transition-1 (Tr_1) to high cGMP (cGMP⊕) to transition-2 (Tr_2) to TUNEL-positive (TU⊕) to dead (D). These stages were represented by a set of differential equations (1–6), to allow calculating the average life-times for each stage as the inverse of the respective decay constant *k*. The values for these equation constants representing the five cell death stages are given in Table 1, together with approximate average life-times and parameter errors. The decay constant k_3 of cGMP⊕ was considerably larger than the decay of the upstream stage Tr_1 (k_2), hence the average life time of cGMP⊕ was governed by k_2, rather than k_3. The model reproduces the progression of cell death as evidenced by cGMP accumulation (sum squared error (SQE) = 0.82), TUNEL assay (SQE = 0.79), and loss of photoreceptor rows (SQE = 0.98). Altogether, the average time for an individual cell to die was predicted to take 83.8 ± 9.4 h (Table 1).

As the loss of photoreceptor cells (Figure 2c) did not follow a strictly exponential decay, we tested an alternative mathematical approach in which k_1 was defined by an asymmetric, generalized logistic function rather than a step function. This may reflect photoreceptor biology in the sense that toward the end of differentiation, the risk for a photoreceptor to die increases dramatically, to then remain constant once full differentiation is reached. Indeed, this approach allowed for a better model fit to cell loss in the initial stage of the degeneration, but in later stages the model fit was not significantly improved (Supplementary Figure 3).

Another, independent estimate of how long the cell death process took, was obtained by plotting data on cGMP accumulation (Figure 2a) together with the derived photoreceptor survival data (Figure 2c) and fitting Gauss curves to

Table 1 Constants and times for the different stages of cell death

Stage	Constant	Value (1/day)	Error (1/day)	Time (h)	Error (h)
H to Tr_1	k_1	0.68	0.06	**35.3**	3.4
cGMP⊕	k_2	0.68	0.07	**35.7**	4.0
cGMP⊕ to Tr_2	k_3	4.24	0.69	**5.6**	0.9
Tr_2 to TU⊕	k_4	5.54	0.98	**4.3**	0.7
TU⊕ to D	k_5	8.19	1.13	**2.9**	0.4

The table gives measures for the average life-times for the five main stages of cell death. The model constants k_1–k_5 were optimized using a Nelder–Mead simplex algorithm, the parameter errors were calculated using the Bootstrapping Algorithm (100 000 samples)

Table 2 Constants of fitted Gauss curves

Constant	Value	Error
f1	0.12	0.01
f2	0.36	0.02
μ1	11.91 d	0.16 d
μ2	13.16 d	0.07 d
σ1	1.02 d	0.07 d
σ2	1.58 d	0.14 d

The table gives the optimized parameters of the two fitted Gauss curves (see Figure 2d). The parameter errors were calculated using the Fisher information matrix[46]

these data sets (Figure 2d, see Table 2 for parameters). The distance between the peaks of the two curves was approximately 30.2 ± 4.9 h and this was interpreted as the average duration of a cell's transit from displaying high levels of cGMP until complete disappearance.

Progression of zaprinast–cGMP-induced cell death. To test and validate the model predictions, we used organotypic retinal explant cultures derived from *wt* animals, exposed to the selective PDE6 inhibitor zaprinast.[20] Zaprinast raises intracellular cGMP levels and induces *wt* photoreceptor degeneration similar to what is seen in *rd1* retina.[12,21] The effects of zaprinast on cGMP levels and TUNEL positivity were investigated at time points ranging from 8 h to 10 d. A significant rise in cGMP-positive cells was detected after 36 h of zaprinast treatment and at all later time points assessed (Figure 3a). Retinal explantation is a traumatic event and the cultures therefore displayed elevated rates of cell death (TUNEL assay) even under control conditions (Figure 3a). This can be regarded as basal level of cell death. Zaprinast caused a significant rise in cell death, but only after 72 h of treatment.

As a result of the culture situation, the number of photoreceptor rows in the ONL *in vitro* is decreasing more strongly than it would *in vivo,* in healthy *wt* retina (Figure 3b). Yet, zaprinast significantly exacerbated this cell loss from 6 d of treatment onward. The delay of almost 36 h between the zaprinast induced rise of cGMP and the rise of cell death another 36 h later corresponded to both the *in vivo* findings and the results of mathematical modeling (Figure 4).

Preservation of cone photoreceptors. In inherited RD in humans, primary rod degeneration is often followed by a secondary, mutation-independent loss of cone photoreceptors. The *rd1* mouse also suffers from such a secondary loss of cones. Zaprinast inhibits both rod and cone PDE6 with similar specificity.[22] To test how zaprinast treatment affected rod and cone photoreceptors, we performed immunostaining for the cone marker glycogen phosphorylase (GP)[23] on retinal cultures after 10 d of zaprinast treatment (i.e., P20). Owing to a somewhat slower retinal development, P20 *in vitro* corresponds to P18 *in vivo*. At P18 in *wt* retina *in vivo*, approximately 5% of ONL cells stained positively for GP. In relative terms cone numbers were far higher in *rd1* retina because of rod loss at this time point *in vivo* (Supplementary Figure 4A, B; quantified in E).

Higher numbers of cones were also found in zaprinast-treated *versus* -untreated *in vitro* retina (Supplementary Figure 4C, D; quantified in E). Even if the relative effect was much smaller than *in vivo*, this suggested that zaprinast-induced degeneration of ONL cells affected mostly rods, particularly when absolute numbers of cones at P18 were considered (Supplementary Figure 4F).

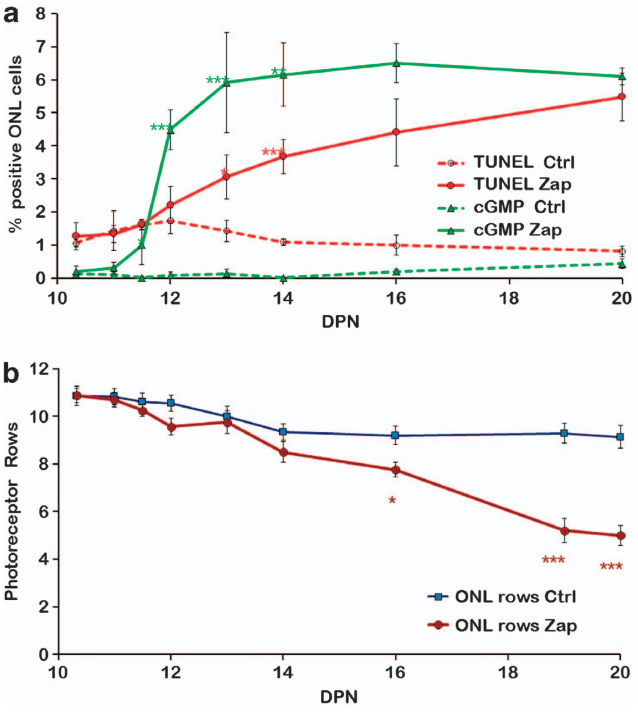

Figure 3 cGMP and photoreceptor degeneration *in vitro*: retinal explant cultures derived from *wt* animals were exposed to the selective PDE6 inhibitor zaprinast (Zap) or control (Ctrl) conditions (**a**). Zap treatment caused an accumulation of cGMP (green curve) only after 36 h, suggesting feedback processes keeping cGMP levels under control initially. The numbers of TUNEL positive, degenerating photoreceptors (red curve) initially remained similar. The number of cGMP-positive cells rose sharply after 36 h of Zap treatment and remained high thereafter. After another 36 h, at P13, the rate of cell death (red curve) increased significantly, a finding that was also reflected in the decreased number of photoreceptor rows (**b**) in Zap-treated (dark red curve) *versus* -untreated specimens. $n = 3$–5 retinae from different *wt* animals; error bars indicate S.E.M.; dotted lines in (**a**) indicate *wt* situation

Discussion

Here, we show for the first time that inherited neuronal cell death in the retina – despite a rapid progression of overall tissue degeneration – is a surprisingly slow process at the level of the individual cell. This affords interesting insights into the underlying mechanism, since a total duration of cell death of approximately 80 h is incompatible with the execution of conventionally assumed necrotic or apoptotic cell death.

cGMP in photoreceptor cell death. High levels of cGMP are known to cause photoreceptor degeneration.[13] In the *rd1* retina accumulation of cGMP is caused by PDE6 dysfunction,[11] and this situation can be replicated by pharmacological inhibition of PDE6.[13,21] The *rd1* mouse seems particularly well suited for studies into the temporal characteristics of cell death, because cGMP accumulation provides a clear label for cell death induction, an event

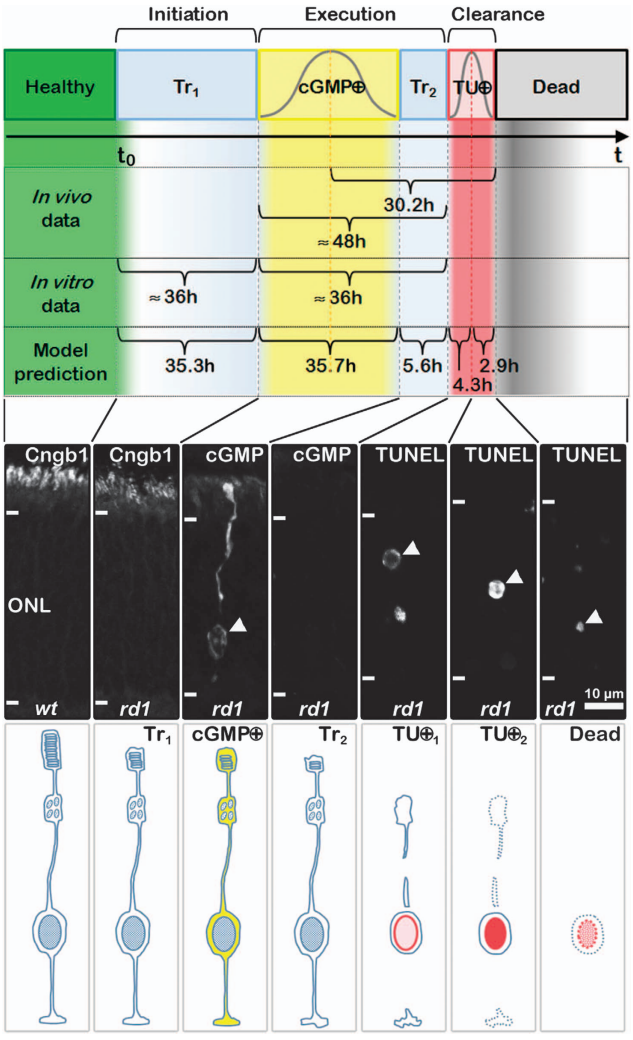

Figure 4 Major phases during neurodegeneration of an individual photoreceptor cell: genetic or pharmacological inactivation of photoreceptor PDE6 initiated cell death. The first transition stage (Tr_1), from the healthy stage to the rise of intracellular cGMP, appeared devoid of specific markers. Yet, it may be associated with decreased outer segment length, as evidenced by staining for cyclic nucleotide channel b1 (Cngb1) in P11 *wt* and *rd1* retina. Both *in vitro* data and modeling suggested that this stage could last around 36 h in total. Tr_1 was followed by the transitory appearance of very high cGMP concentrations (cGMP ⊕), a stage that may have lasted another 36 h, and possibly marked the beginning of cell death execution. High cGMP was followed by a second transition stage (Tr_2), which took about 5–6 h and was negative for both cGMP and the TUNEL assay. The ensuing DNA fragmentation then caused the cell to turn TUNEL positive (TU ⊕), first in the nuclear periphery, then in the entire nucleus, which finally became very small, pyknotic, before it disappeared. This final stage – the clearance phase – from the beginning of a positive reaction in the TUNEL assay to the complete clearance of the cell, lasted another 6–7 h. Together, *in vivo* and *in vitro* data, as well as modeling, proposed ≈80 h for the total duration of an individual cell's death, a time frame that is remarkably long and axiomatically incompatible with execution of either necrosis or apoptosis

otherwise difficult to assess. cGMP has two prototypic targets: cGMP-dependent protein kinase G (PKG)[12] and cyclic nucleotide gated (CNG) channels.[24] In photoreceptors, cGMP levels are controlled by a physiologic feedback mechanism via activation of CNG channels, resulting in Ca^{2+} influx, which in turn inhibits guanylyl cyclase (GC) and cGMP production.[25,26] Why this control mechanism fails to keep cGMP in check after prolonged elevation of cGMP is unknown, but may be linked to cGMP-dependent activation of PKG[12] and its effects on gene regulation.[27] Indeed, extensive gene expression changes were seen in *rd1* retina already at P11.[28] At the same time, excessively high cGMP-levels may precipitate *rd1* cell death via over-activation of CNG channels and subsequent influx of Ca^{2+} ions.[29,30]

Cell death mechanisms. A variety of different mechanisms have been connected with neuronal cell death,[3,14] but necrosis and apoptosis are possibly the best well known and often seen as conceptual counterparts. While necrosis usually is very rapid, taking no more than a few hours to complete,[3] apoptosis is somewhat slower, requiring 6–18 h typically.[6,7] Characteristic features of necrosis not seen in apoptosis are activation of the immune system and an inflammation, as well as necrotic clumping of dying cells. Photoreceptor cell death during primary RD is topologically independent and generally there is no evidence for inflammation,[16] although an upregulation of innate immunity[31] and secondary infiltration of microglial cells into the ONL has been reported.[32] Both *rd1* and *wt* retina show small numbers of cells with activated caspase-3 – a key feature of apoptosis and likely related to early post-natal developmental cell death.[20] However, *rd1* mutation-induced cell death is caspase-independent and devoid of classical apoptotic features.[16] It is tempting to speculate that instead of necrosis or apoptosis, we may be facing an alternative cell death mechanism,[3] possibly involving metabolic activities of PKG,[12] histone deacetylase (HDAC),[33] poly-ADP-ribose polymerase (PARP),[28] and calpains.[34] Our data indicate that this form of cell death is considerably more time consuming than both necrosis and apoptosis. This is in line with findings in caspase-deficient neurons suggesting that caspase-independent cell death may be slower than caspase-mediated apoptosis.[35] An alternative explanation for the exceptionally slow progression observed here, could be that – maybe in the initial phases – the execution of cell death is counteracted by endogenous survival mechanisms.[36]

The kinetics of photoreceptor death. Rod photoreceptors in the mouse are born over a 16-d period ranging from 7 d before to 9 d after birth,[37] and one could hypothesize that the lifespan of *rd1* photoreceptors might be constant and predetermined by their respective date of birth. On the other hand, *rd1* photoreceptor degeneration at the tissue level is governed by a constant rate of cell death and first-order kinetics,[17] with one cell's death entirely independent from another cell's death. This is very similar to what is observed in the exponential decay of radioactive elements and hence, the lifespan of an individual photoreceptor cell will be random and governed by probabilistic and stochastic effects.[38] In this model, the average life-span of a cell population will be governed by the severity of the (genetic) insult.[18]

The kinetics of cell death presented here are generally compatible with the 'one-hit-model'.[17] We introduced several novel parameters to this model, including different cell death stages and a variable risk for the initial stage. Indeed, we found that an individual *rd1* photoreceptor's risk to die may

increase during early post-natal differentiation and reach a constant value only once the fully differentiated state is reached. This would result in an apparent wave of cell death at the time of differentiation and may serve to explain the center to periphery progression of the *rd1* degeneration, which follows the pattern of retinal development.

Zaprinast treatment: simulation of an inherited disease?. Studies of inherited RDs can be helped by disease simulation on different genetic backgrounds or in different species. Pioneering works by Lolley *et al.*[13] used the general PDE inhibitor 3-isobutyl-1-methylxanthine to pharmacologically induce selective, cGMP-dependent photoreceptor degeneration in *Xenopus* embryos. In mammalian systems, zaprinast is a highly selective PDE6 inhibitor,[22] which – as used here (100 μM) – causes cGMP accumulation and exclusive photoreceptor death.[12,21] Interestingly, and very similar to the *in vivo* characteristics of the *rd1* retina, zaprinast affected sub-populations of photoreceptor cells at different times, which also *in vitro* might be connected to ongoing development of photoreceptors,[37] superseded by stochastic effects.[38]

Unexpectedly, the dramatic rise of photoreceptor cGMP levels was not an immediate effect of zaprinast treatment. Although zaprinast increases Ca^{2+}-levels cGMP dependently in mouse photoreceptors within minutes of application,[39] a catastrophic rise of cellular cGMP to levels detectable with immunostaining appeared only after 36 h and beyond. These non-linear kinetics of cGMP accumulation suggest that feedback control mechanisms, such as the CNG-Ca^{2+}-GC loop,[25] prevent the rise of cGMP for approximately 1.5 d, before a changing metabolism causes cGMP levels to go unchecked.

Contrary to what might be expected from its inhibitory capacity on both rod and cone PDE6 isoforms,[20] zaprinast did not seem to affect cones. This may point at an increased resistance of cones to higher cGMP levels[40] but could also be due to their later differentiation.[41] Anyhow, within the time frame of our experiments, *in vitro* application of zaprinast on wt retina faithfully reproduced the selective rod photoreceptor loss seen in *rd1* retina *in vivo*. This approach could prove very useful to study retinal neurodegenerative mechanisms, for instance on non-degenerating knock-out rodent models[21] or on large, non-rodent animal models.

The slow death of photoreceptors: three phases in cell death. Our different experimental approaches delineate three major phases in the progression of cell death and give estimates on their duration (Figure 4).

1. *The initiation phase*: this phase of cell death is inherently difficult to study because of our lack of understanding of relevant metabolic processes and suitable markers. Nevertheless, both *in vivo* and *in vitro* data suggested that after inhibition or genetic inactivation of PDE6, cGMP levels rise but are maintained within physiological limits by feedback control mechanisms.[25] Possibly, the cell is not yet committed to die at this stage, although toward its end the feedback control is shut down and cGMP rises beyond physiological limits. PKG is involved in the degeneration[12] and has a 100-fold higher sensitivity to cGMP compared with CNG channels.[42] PKG could therefore have a preeminent role during this phase, which our data suggest takes about 36 h.
2. *The execution phase*: once the cellular metabolism has switched to allow for a catastrophic rise of cGMP, the cell likely becomes committed to die and enters the death execution phase. This phase may be characterized by an over-activation of HDAC[33] and subsequently PARP,[28] resulting in chromatin changes and rearrangements. In addition, high cGMP likely acts on CNG channels,[30] to cause excessive Ca^{2+} influx[29] and calpain activation.[34] The execution phase may last between 36 and 48 h. Similarly, chick embryo neuronal precursor cells became committed to die approximately 2 d before clear signs of impending cell death were observed.[6]
3. *The clearance phase*: once the cell has reached the final stages of cell death, extensive DNA fragmentation sets in, as evidenced by the TUNEL assay. It is worth mentioning that the TUNEL assay generally labels dying cells, including in necrosis[19] and apoptosis.[2] Our model suggests that it may take about 4 h until a maximal degree of DNA fragmentation is reached, and from then on the nucleus becomes more and more condensed and pyknotic until the cellular debris is completely removed, a stage that may take another 3 h. This is in agreement with studies on clearance of TUNEL-positive cells in rat and mouse neocortex, estimated to last between 1 and 4 h,[10] and clearance of pyknotic ganglion cells during retinal development within 1 h.[43]

Even with cautious extrapolation to the human situation, where RD caused by homologous mutations may take several decades to complete, the observed delays suggest a window-of-opportunity sufficiently large for therapeutic interventions in patients. They also confirm previous observations that photoreceptor metabolism may suffer significantly before evident cell loss leads to first clinical symptoms.[44] With respect to potential neuroprotective treatments, targeting of metabolic processes[36] during initiation or early execution phases may be particularly promising.

Conclusion

Our study for the first time provides consistent estimates on the duration of neuronal cell death in a hereditary neurodegenerative disease. With a period of about 80 h – from initiation, to cGMP accumulation, to TUNEL-positive reaction, to clearance – the time an individual cell needs to die is remarkably long and points toward execution of non-necrotic, non-apoptotic, and relatively slow cell death mechanisms. This has clear relevance for the development of potential therapies, for instance in acute neurodegenerative disorders such as stroke or spinal-cord injury, where the time frame for cell death will directly determine the window-of-opportunity and potential therapeutic options. Similarly, for chronic and inherited forms of neurodegeneration, knowledge on the temporal progression of cell death will provide insights into the underlying degenerative mechanisms and again define possible treatment approaches.

The mathematical model presented here may be extended to also include other processes causally involved in cell death, such as enzymatic activities of PKG, HDAC, PARP, and calpain. Combined with the use of transgenic biosensors for cGMP and Ca^{2+},[39] this could allow precise delineation of the temporal progression and interdependence of different metabolic processes causing cell death. Furthermore, the current experimental approach and type of mathematical modeling may be used to study cell death in general, provided at least two temporally distinct degeneration markers can be identified.

Materials and Methods

Animals. C3H *rd1*/*rd1* (*rd1*) and control C3H *wt* mice were housed under standard white cyclic lighting, had free access to food and water, and were used irrespective of gender. All procedures were performed in accordance with the local ethics committee at Tübingen University (§4 registration from 23 January 2008), and the ARVO statement for the use of animals in ophthalmic and visual research. All efforts were made to minimize the number of animals used and their suffering. Day of birth was considered as post-natal day (P) 0.

Organotypic retinal explant culture. Retinae from P5 *rd1* and *wt* animals were used to generate retinal explants as described before.[21,33] Explanted retinae were cultured on Millicell HA culture dish filter inserts (Millipore, Carrigtwohill, Cork, Ireland; PIHA03050) with the retinal pigment epithelium facing the membrane. Inserts were put into six-well culture plates and incubated in R16 nutrient medium with supplements at 37 °C. Every second day the full volume of nutrient medium, 1.5 ml per well, was replaced with fresh medium. After 5 d *in vitro* (i.e., P10), the two retinal explants obtained from one animal were split into two groups, one was exposed to 100 μM zaprinast in DMSO (treatment group), one was exposed to DMSO only (control group; 0.3% DMSO). The culture period was ended by immediate fixation in 4% paraformaldehyde in PBS at post-treatment time points ranging from 8 h to 10 d.

Immunostaining and TUNEL assay. Retinal cryosections obtained either from *in vivo* animals or following *in vitro* explant culture, were dried for 30–60 min at 37 °C. Subsequently, the tissue was rehydrated in PBS, and pre-incubated for 1 h at room temperature in blocking solution, containing 10% normal serum, and 0.1% or 0.3% Triton in PBS (PBST). Immunostaining was performed overnight at 4 °C, using primary antibodies against cGMP (provided by Harry Steinbusch, Maastricht University, The Netherlands), Cngb1 (provided by Stylianos Michalakis, Ludwig Maximilian University of Munich, Germany), and GP (provided by Brigitte Pfeiffer-Gugliemi, University of Tübingen, Germany) diluted 1 : 500 in blocking solution. The tissue was rinsed with PBST, and incubated for 1 h with a corresponding, Alexafluor-488 conjugated, secondary antibody (1 : 200–1 : 750, Life technologies, Darmstadt, Germany), diluted in PBST. Sections were rinsed in PBS, and mounted in Vectashield with DAPI for nuclear counterstaining (Vector Laboratories Inc., Burlingame, CA, USA). The TUNEL assay was performed on using an *in situ* cell death detection kit conjugated with tetra-methyl-rhodamine or fluorescein isothiocyanate (Roche Diagnostics, Mannheim, Germany). For controls terminal deoxynucleotidyl transferase enzyme was either omitted from the labeling solution (negative control), or sections were pre-treated for 30 min with DNAse I (Roche, 3 U/ml) in 50 mM Tris-HCl, pH 7.5, 1 mg/ml BSA to induce DNA strand breaks (positive control). Although negative control gave no staining, positive control stained all nuclei in all layers of the retina.[28]

Microscopy, cell counting, and statistical analysis. Morphological observations and routine light microscopy were performed on a Zeiss Imager Z1 Apotome Microscope (Zeiss, Oberkochen, Germany), equipped with a Zeiss Axiocam digital camera. Images were captured using Zeiss Axiovision 4.8 software; image overlays and contrast enhancement were done using Adobe Photoshop CS5. Images shown in figures are representative for least three different animals for each genotype/treatment. Percentages of TUNEL-positive cells were assessed in a blinded fashion as reported previously.[33,34] The mean value for photoreceptor rows in the ONL was determined using DAPI staining on six different locations in close proximity to the optic nerve (*in vivo*) or in central areas of the retinal explant (*in vitro*). To generate the data set for dead cells and to account for early post-natal developmental cell death, the *wt* photoreceptor row count was subtracted from the respective *rd1* values. Values are mean ± S.E.M. Statistical significance was tested using one-way ANOVA with Bonferroni correction and GraphPad Prism 5 software (San Diego, CA, USA), significance levels were: $^{*}P<0.05$, $^{**}P<0.01$, and $^{***}P<0.001$.

Mathematical models. For modeling cell death progression and estimating its duration, irreversible first-order kinetics were assumed.[17] The model consisted of six stages, termed 'healthy'(H), 'transition state-1' (Tr_1), 'cGMP-positive' (cGMP$\oplus$), 'transition state-2' (Tr_2), 'TUNEL-positive' (TU$\oplus$) and 'dead' (D). The changes in the six stages are represented by an ordinary differential equation system:

$$\frac{\mathrm{d}}{\mathrm{d}t}H(t) = -k_1 \cdot H(t) \tag{1}$$

$$\frac{\mathrm{d}}{\mathrm{d}t}\mathrm{Tr}_1(t) = k_1 \cdot H(t) - k_2 \cdot \mathrm{Tr}_1(t) \tag{2}$$

$$\frac{\mathrm{d}}{\mathrm{d}t}\mathrm{cGMP}\oplus(t) = k_2 \cdot \mathrm{Tr}_1(t) - k_3 \cdot \mathrm{cGMP}\oplus(t) \tag{3}$$

$$\frac{\mathrm{d}}{\mathrm{d}t}\mathrm{Tr}_2(t) = k_3 \cdot \mathrm{cGMP}\oplus(t) - k_4 \cdot \mathrm{Tr}_2(t) \tag{4}$$

$$\frac{\mathrm{d}}{\mathrm{d}t}\mathrm{TU}\oplus(t) = k_4 \cdot \mathrm{Tr}_2(t) - k_5 \cdot \mathrm{TU}\oplus(t) \tag{5}$$

$$\frac{\mathrm{d}}{\mathrm{d}t}D(t) = k_5 \cdot \mathrm{TU}\oplus(t) \tag{6}$$

k_1, k_2, k_3, k_4, and k_5 stand for the decay constants of the respective equation and cell death stage (see additional considerations in results). The average life-time τ_x of a given cell death stage x will be the inverse of the respective decay constant k_x. This model was implemented in Matlab 2010a (Mathworks, Natick, MA, USA). The system of differential equations was solved using 'ode45' algorithm (explicit Runge–Kutta based).

$$\tau_x = \frac{1}{k_x} \tag{7}$$

The SQE was calculated using equation (8) where y represents the measured values of healthy, cGMP-positive, TUNEL-positive and dead cells stages, y^p represents predicted values of these variables, whereas n stands for the total number of observations. For the SQE calculation, we summed the predicted values for the healthy the Tr_1 state, because these two states were indistinguishable experimentally.

$$\mathrm{SQE} = \sum_{i=0}^{n} \left(y_i - y_i^p\right)^2 \tag{8}$$

To fit the parameters, we used the Nelder–Mead Simplex Algorithm ('fminsearch') to minimize SQE, and to match the model as closely as possible to the observed cell death processes. Initially, decay constants and starting time t_0 of the system of differential equations were part of the optimization and subsequent bootstrapping. From the probability density function of possible start times, we choose the time with the highest probability below 10 d post-natal, which was 9.84 d. For biological reasons, solutions beyond 10 d were not considered. The final parameters were then optimized with a fixed starting time t_0 of 9.84 d.

To model the continuous decay of the healthy stage, an extension of the above described model was tested, which used a generalized logistic function equation (9) instead of a constant $k1$ (Supplementary Figure 4). The simulation of this model and estimation of the generalized logistic functioń s parameters were performed using COPASI – software[45] and the simulated annealing algorithm for parameter estimation. The decay constants k_2–k_5 were left unchanged.

$$k_1(t) = A + \frac{K - A}{\left(1 + Q \cdot e^{-B(t-M)}\right)^{1/v}} \tag{9}$$

An alternative, empirical approach is given in a second model, which provides an estimate of the 'life-time' of the sick (S) state of a cell (i.e., the cell death execution phase). The 'life-time' of the sick cells Δt was assumed to be the time t_2 (peak of cell death) minus the time t_1 (peak of cGMP-positive cells). To estimate the time point t_1 with the maximum number of cells that are in the sick state $S(t)$, a Gauss function equation (10) was fitted to the normalized cGMP$\oplus$ data peak, where f_1 is a parameter for peak height and σ_1 represents peak width. The maximal increase in dead cells was determined in the same way by fitting a Gauss function equation (11) to the derivative of the dead cell data. Δt equation (12) gives the average life-time of

sick cells.

$$S(t) \approx \frac{f_1}{\sigma_1} e^{-\frac{1}{2}((t-t_1)/\sigma_1)^2} \quad (10)$$

$$\frac{\mathrm{d}}{\mathrm{d}t} D(t) \approx \frac{f_2}{\sigma_2} e^{-\frac{1}{2}((t-t_2)/\sigma_2)^2} \quad (11)$$

$$\Delta t = t_2 - t_1 \quad (12)$$

The second model was realized in Microsoft Excel 2010 (Microsoft, Unterschleissheim, Germany) using the 'Solver' functionality with genetic algorithms and SQE to fit the functions to the measured data.

Conflict of Interest

The authors declare no conflict of interest.

Acknowledgements. We thank T Euler, B Arango-Gonzalez and D Trifunović for helpful comments and discussions. This work was supported by grants from DFG (Pa1751/4-1, 1-1), and Open Access Publishing Fund of Tuebingen University, EU (DRUGSFORD: HEALTH-F2-2012-304963), CIN (PP2009-20), and Kerstan Foundation.

1. Kerr JF, Wyllie AH, Currie AR. Apoptosis: a basic biological phenomenon with wide-ranging implications in tissue kinetics. *Br J Cancer* 1972; **26**: 239–257.
2. Gavrieli Y, Sherman Y, Ben-Sasson SA. Identification of programmed cell death in situ via specific labeling of nuclear DNA fragmentation. *J Cell Biol* 1992; **119**: 493–501.
3. Zong WX, Thompson CB. Necrotic death as a cell fate. *Genes Dev* 2006; **20**: 1–15.
4. Henson PM, Hume DA. Apoptotic cell removal in development and tissue homeostasis. *Trends Immunol* 2006; **27**: 244–250.
5. Skommer J, Darzynkiewicz Z, Wlodkowic D. Cell death goes LIVE: technological advances in real-time tracking of cell death. *Cell Cycle* 2010; **9**: 2330–2341.
6. Oppenheim RW. Cell death during development of the nervous system. *Annu Rev Neurosci* 1991; **14**: 453–501.
7. Wong RO, Hughes A. Role of cell death in the topogenesis of neuronal distributions in the developing cat retinal ganglion cell layer. *J Comp Neurol* 1987; **262**: 496–511.
8. Cordeiro MF, Guo L, Coxon KM, Duggan J, Nizari S, Normando EM *et al.* Imaging multiple phases of neurodegeneration: a novel approach to assessing cell death *in vivo*. *Cell Death Dis* 2010; **1**: e3.
9. Alborzinia H, Can S, Holenya P, Scholl C, Lederer E, Kitanovic I *et al.* Real-time monitoring of cisplatin-induced cell death. *PLoS ONE* 2011; **6**: e19714.
10. Gohlke JM, Griffith WC, Faustman EM. The role of cell death during neocortical neurogenesis and synaptogenesis: implications from a computational model for the rat and mouse. *Brain Res Dev Brain Res* 2004; **151**: 43–54.
11. Bowes C, Li T, Danciger M, Baxter LC, Applebury ML, Farber DB. Retinal degeneration in the rd mouse is caused by a defect in the beta subunit of rod cGMP-phosphodiesterase. *Nature* 1990; **347**: 677–680.
12. Paquet-Durand F, Hauck SM, van Veen T, Ueffing M, Ekström P. PKG activity causes photoreceptor cell death in two retinitis pigmentosa models. *J Neurochem* 2009; **108**: 796–810.
13. Lolley RN, Farber DB, Rayborn ME, Hollyfield JG. Cyclic GMP accumulation causes degeneration of photoreceptor cells: simulation of an inherited disease. *Science* 1977; **196**: 664–666.
14. Chang GQ, Hao Y, Wong F. Apoptosis: final common pathway of photoreceptor death in rd, rds, and rhodopsin mutant mice. *Neuron* 1993; **11**: 595–605.
15. Trichonas G, Murakami Y, Thanos A, Morizane Y, Kayama M, Debouck CM *et al.* Receptor interacting protein kinases mediate retinal detachment-induced photoreceptor necrosis and compensate for inhibition of apoptosis. *Proc Natl Acad Sci USA* 2010; **107**: 21695–21700.
16. Sancho-Pelluz J, Arango-Gonzalez B, Kustermann S, Romero FJ, van Veen T, Zrenner E *et al.* Photoreceptor cell death mechanisms in inherited retinal degeneration. *Mol Neurobiol* 2008; **38**: 253–269.
17. Clarke G, Collins RA, Leavitt BR, Andrews DF, Hayden MR, Lumsden CJ *et al.* A one-hit model of cell death in inherited neuronal degenerations. *Nature* 2000; **406**: 195–199.
18. Wright AF, Chakarova CF, Abd El-Aziz MM, Bhattacharya SS. Photoreceptor degeneration: genetic and mechanistic dissection of a complex trait. *Nat Rev Genet* 2010; **11**: 273–284.
19. Grasl-Kraupp B, Ruttkay-Nedecky B, Koudelka H, Bukowska K, Bursch W, Schulte-Hermann R. In situ detection of fragmented DNA (TUNEL assay) fails to discriminate among apoptosis, necrosis, and autolytic cell death: a cautionary note. *Hepatology* 1995; **21**: 1465–1468.
20. Young RW. Cell death during differentiation of the retina in the mouse. *J Comp Neurol* 1984; **229**: 362–373.
21. Sahaboglu A, Tanimoto N, Kaur J, Sancho-Pelluz J, Huber G, Fahl E *et al.* PARP1 gene knock-out increases resistance to retinal degeneration without affecting retinal function. *PLoS ONE* 2010; **5**: e15495.
22. Zhang X, Feng Q, Cote RH. Efficacy and selectivity of phosphodiesterase-targeted drugs in inhibiting photoreceptor phosphodiesterase (PDE6) in retinal photoreceptors. *Invest Ophthalmol Vis Sci* 2005; **46**: 3060–3066.
23. Nihira M, Anderson K, Gorin FA, Burns MS. Primate rod and cone photoreceptors may differ in glucose accessibility. *Invest Ophthalmol Vis Sci* 1995; **36**: 1259–1270.
24. Huttl S, Michalakis S, Seeliger M, Luo DG, Acar N, Geiger H *et al.* Impaired channel targeting and retinal degeneration in mice lacking the cyclic nucleotide-gated channel subunit CNGB1. *J Neurosci* 2005; **25**: 130–138.
25. Olshevskaya EV, Ermilov AN, Dizhoor AM. Factors that affect regulation of cGMP synthesis in vertebrate photoreceptors and their genetic link to human retinal degeneration. *Mol Cell Biochem* 2002; **230**: 139–147.
26. Michalakis S, Mühlfriedel R, Tanimoto N, Krishnamoorthy V, Koch S, Fischer MD *et al.* Restoration of cone vision in the CNGA3(-/-) mouse model of congenital complete lack of cone photoreceptor function. *Mol Ther* 2010; **18**: 2057–2063.
27. Fiscus RR. Involvement of cyclic GMP and protein kinase G in the regulation of apoptosis and survival in neural cells. *Neurosignals* 2002; **11**: 175–190.
28. Paquet-Durand F, Silva J, Talukdar T, Johnson LE, Azadi S, van Veen T *et al.* Excessive activation of poly(ADP-ribose) polymerase contributes to inherited photoreceptor degeneration in the retinal degeneration 1 mouse. *J Neurosci* 2007; **27**: 10311–10319.
29. Fox DA, Poblenz AT, He L. Calcium overload triggers rod photoreceptor apoptotic cell death in chemical-induced and inherited retinal degenerations. *Ann N Y Acad Sci* 1999; **893**: 282–285.
30. Paquet-Durand F, Beck S, Michalakis S, Goldmann T, Huber G, Mühlfriedel R *et al.* A key role for cyclic nucleotide gated (CNG) channels in cGMP-related retinitis pigmentosa. *Hum Mol Genet* 2011; **20**: 941–947.
31. Azadi S, Paquet-Durand F, Medstrand P, van Veen T, Ekström PA. Up-regulation and increased phosphorylation of protein kinase C (PKC) delta, mu and theta in the degenerating rd1 mouse retina. *Mol Cell Neurosci* 2006; **31**: 759–773.
32. Murakami Y, Matsumoto H, Roh M, Suzuki J, Hisatomi T, Ikeda Y *et al.* Receptor interacting protein kinase mediates necrotic cone but not rod cell death in a mouse model of inherited degeneration. *Proc Natl Acad Sci USA* 2012; **109**: 14598–14603.
33. Sancho-Pelluz J, Alavi MV, Sahaboglu A, Kustermann S, Farinelli P, Azadi S *et al.* Excessive HDAC activation is critical for neurodegeneration in the rd1 mouse. *Cell Death Disease* 2010; **1**: 1–9.
34. Paquet-Durand F, Sanges D, McCall J, Silva J, van Veen T, Marigo V *et al.* Photoreceptor rescue and toxicity induced by different calpain inhibitors. *J Neurochem* 2010; **115**: 930–940.
35. Oppenheim RW, Flavell RA, Vinsant S, Prevette D, Kuan CY, Rakic P. Programmed cell death of developing mammalian neurons after genetic deletion of caspases. *J Neurosci* 2001; **21**: 4752–4760.
36. Trifunovic D, Sahaboglu A, Kaur J, Mencl S, Zrenner E, Ueffing M *et al.* Neuroprotective strategies for the treatment of inherited photoreceptor degeneration. *Curr Mol Med* 2012; **12**: 598–612.
37. Cepko CL, Austin CP, Yang X, Alexiades M, Ezzeddine D. Cell fate determination in the vertebrate retina. *Proc Natl Acad Sci USA* 1996; **93**: 589–595.
38. Skommer J, Raychaudhuri S, Wlodkowic D. Timing is everything: stochastic origins of cell-to-cell variability in cancer cell death. *Front Biosci* 2011; **16**: 307–314.
39. Wei T, Schubert T, Paquet-Durand F, Tanimoto N, Chang L, Koeppen K *et al.* Generation and functional characterization of a transgenic mouse expressing a Ca2 + biosensor in cone photoreceptors. *J Neurosci* 2012; **32**: 6994–6981.
40. Johnson JE Jr, Perkins GA, Giddabasappa A, Chaney S, Xiao W, White AD *et al.* Spatiotemporal regulation of ATP and Ca2 + dynamics in vertebrate rod and cone ribbon synapses. *Mol Vis* 2007; **13**: 887–919.
41. Szél Á, van Veen T, Röhlich P. Retinal cone differentiation. *Nature* 1994; **370**: 336.
42. Lincoln TM, Cornwell TL. Intracellular cyclic GMP receptor proteins. *FASEB J* 1993; **7**: 328–338.
43. Cellerino A, Galli-Resta L, Colombaioni L. The dynamics of neuronal death: a time-lapse study in the retina. *J Neurosci* 2000; **20**: RC92.
44. Acosta ML, Shin YS, Ready S, Fletcher EL, Christie DL, Kalloniatis M *et al.* Retinal metabolic state of the proline-23-histidine rat model of retinitis pigmentosa. *Am J Physiol Cell Physiol* 2010; **298**: C764–C774.
45. Hoops S, Sahle S, Gauges R, Lee C, Pahle J, Simus N *et al.* COPASI- A COmplex PAthway SImulator. *Bioinformatics* 2006; **22**: 3067–3074.
46. Lindner O, Hitzmann B. Experimental design for optimal parameter estimation of an enzyme kinetic process based on the analysis of the Fisher information matrix. *J Theor Biol* 2006; **238**: 111–123.

Supplementary Information accompanies the paper on Cell Death and Disease website (http://www.nature.com/cddis)